

# A Plasma Instability Theory of Gamma-Ray Burst Emission

J. J. Brainerd<sup>1</sup>

University of Alabama in Huntsville

## ABSTRACT

A plasma instability theory is presented for the prompt radiation from gamma-ray bursts. In the theory, a highly relativistic shell interacts with the interstellar medium through the filamentation and the two-stream instabilities to convert bulk kinetic energy into electron thermal energy and magnetic field energy. The processes are not efficient enough to satisfy the Rankine-Hugoniot conditions, so a shock cannot form through this mechanism. Instead, the interstellar medium passes through the shell, with the electrons radiating during this passage. Gamma-rays are produced by synchrotron self-Compton emission. Prompt optical emission is also produced through this mechanism, while prompt radio emission is produced through synchrotron emission. The model timescales are consistent with the shortest burst timescales. To emit gamma-rays, the shell's bulk Lorentz factor must be  $\gtrsim 10^3$ . For the radiative processes to be efficient, the interstellar medium density must satisfy a lower limit that is a function of the bulk Lorentz factor. Because the limits operate as selection effects, bursts that violate them constitute new classes. In particular, a class of optical and ultraviolet bursts with no gamma-ray emission should exist. The lower limit on the density of the interstellar medium is consistent with the requirements of the Compton attenuation theory, providing an explanation for why all burst spectra appear to be attenuated. Several tests of the theory are discussed, as are the next theoretical investigations that should be conducted.

*Subject headings:* Gamma rays: bursts

## 1. Overview

Current observations of gamma-ray bursts place a number of strong constraints on gamma-ray burst physics. The measured red shift of  $z = 0.835$ ,  $0.966$ , and  $1.61$  for lines in the optical emission of gamma-ray bursts GRB 970508 (Metzger et al. 1997a,b), GRB 980703 (Djorgovski et al. 1998a,b), and GRB 990123 (Kelson et al. 1999), respectively, and the indirect redshifts

---

<sup>1</sup>Space Sciences Lab, ES-84, NASA/Marshall Space Flight Center, Huntsville, AL 35812  
Jim.Brainerd@msfc.nasa.gov

of  $z = 3.5$ ,  $5$ , and  $1.096$  for GRB 971214 (Kulkarni, S. R., et al. 1998), GRB 980329 (Fruchter 1999), and GRB 980613 (Djorgovski et al. 1999), respectively, show that gamma-ray bursts are at extraordinarily-high redshifts. The power-law gamma-ray spectrum above  $511$  keV and the rapid rise times of the gamma-ray light-curves force one to consider theories with highly-relativistic bulk motion in order to avoid thermalization of the gamma-rays through photon-photon pair creation (Schmidt 1978; Baring, & Harding 1996). The gamma-ray spectrum can be characterized by the E-peak energy ( $E_p$ ), which is the photon energy of the maximum of the  $\nu F_\nu$  spectrum. Because the distribution of  $E_p$  values is narrow, with an average value of  $E_p \approx 250$  keV (Mallozzi et al. 1996; Brainerd et al. 1999), one suspects that the characteristics of the spectrum are independent of the bulk Lorentz factor, which should vary greatly from burst to burst. In some bursts, the shape of the gamma-ray spectrum is inconsistent with optically thin synchrotron emission (Preece et al. 1998a,b). The shape of the burst spectrum is consistent with being Compton attenuated by a high density ( $\approx 10^5$  cm $^{-3}$ ) interstellar medium (Brainerd 1994; Brainerd et al. 1996,1998); observations show the x-ray excess predicted by this theory (Preece et al. 1996), and the redshifts of  $\approx 1$  to  $\approx 10$  derived by fitting the model to burst spectra are consistent with the values measured at optical wavelength (Preece & Brainerd 1999). The success of this theory, its presence in every gamma-ray burst, implies that a high density interstellar medium is necessary for a burst to occur.

The observations suggest that the sources of gamma-ray bursts are compact—perhaps a several mass black hole, perhaps a supermassive black hole—and that these sources eject mass at relativistic velocities in one short event. The observed behavior of the gamma-ray burst arises from processes that convert the kinetic energy of the ejected material into electromagnetic radiation.

The general view that has developed concerning the gamma-ray emission of gamma-ray bursts is that it is radiated behind a shock that has developed within a shell moving with a bulk Lorentz factor of  $\Gamma \approx 10^3$  (Mészáros 1998). The radiative mechanism universally cited is synchrotron emission from electrons accelerated to an energy close to the equipartition energy (Tavani 1996). The shock itself is collisionless, arising either when the shell runs into the interstellar medium, or when the fastest portions of the shell overtake slower portions (Rees & Mesaros 1992, 1994; Piran & Sari 1998; Mochkovitch & Daigne 1998). This model has several shortcomings. First, the gamma-ray burst spectrum is often harder at x-ray energies than is allowed by an optically-thin synchrotron emission model. Second, it provides no explanation for the x-ray excess, for the narrow  $E_p$  distribution, or for the apparent absence of bursts with  $\Gamma < 10^3$ , as inferred from the absence of photon-photon pair creation and thermalization. From the theoretical side, many assumptions are made without theoretical development; among these are that collective processes exist that mediate the shock, that a strong magnetic field is generated in the shock, and that the energy is efficiently transferred from the bulk-motion of the ions to the thermal energy of the electrons.

It is with these difficulties in mind that a new theory for the generation of the prompt radiation in a gamma-ray burst is proposed. The theory is a plasma instability theory. In

this theory, the shell of relativistic material that is ejected from the source interacts with the interstellar medium through the plasma filamentation instability, which, in the relativistic regime, has a higher growth rate than the two-stream instability. Because the mass ejection event must be short, of order the burst durations, and because the mass travels  $2c\Gamma^2$  times the burst duration, the interaction is of a thin shell with the interstellar medium. As the shell passes through the interstellar medium, the interstellar medium collapses into filaments that contain strong magnetic fields and high electron thermal energies. It is the interstellar medium that filaments rather than the shell, because the interstellar medium has the smaller density as measured in each comoving reference frame. The ions in the filaments remain essentially at rest with respect to the observer, while the electrons move towards the observer with a high bulk Lorentz factor. The magnetic fields generated through filamentation are strong enough to produce gamma-rays through synchrotron self-Compton emission. One finds that the theory places lower limits on both  $\Gamma$  and the interstellar medium density through selection effects, and that these lower limits lead to the conditions required by the Compton attenuation theory. The theory implies that there exists a class of burst that produces intense and prompt optical and ultraviolet emission, but no x-rays and gamma-rays.

In this article, I give an analytic development of the theory outlined above. This development explores the relevant plasma and radiative processes, deriving the selection effects inherent in the theory, and ascertaining the aspects of the theory that provide means of observationally testing the theory. In §2, the characteristic ratio of shell density to interstellar medium density and the characteristic thickness of the shell are discussed. In §3, the growth of the two-stream and filamentation plasma instabilities is examined. The saturation of the filaments and the inability of the filamentation instability to mediate a shock are examined in §4. The electron thermalization and isotropization and the rest frame defined by the electron component are discussed in §5. The radiative processes of synchrotron emission and synchrotron self-Compton emission are examined in §6, where the characteristic frequencies and emission rates of each are derived. In §7, the radiative timescales for synchrotron and synchrotron self-Compton cooling are derived. The theory has several natural selection effects that constrain several of the free parameters in the theory. These are discussed in §8. The basic theory and the results of this study are summarized in §9. This section also contains some suggestions for observational tests of the validity of the theory.

## 2. Characteristic Model Parameters

The model is of a fully-ionized neutral shell of electrons and protons passing through a fully-ionized interstellar medium of electrons and protons. The characteristic physical parameters that describe this theory are  $n_{ism}$ , the number density of the electrons or of the protons in the interstellar material,  $n'_{shell}$ , the number density of the electrons or protons in the relativistic shell, and  $\Gamma$ , the Lorentz factor of the shell relative to the interstellar medium. The quantities with primes are measured in the shell rest frame, while those without primes are measured in the interstellar medium rest frame. An important parameter in the discussion that follows is the

parameter  $\eta$ , defined as

$$\eta = \frac{n_{ism}}{n'_{shell}}. \quad (1)$$

There is no simple connection between  $\eta$ ,  $\Gamma$ , and the parameters that describe the energetics of the system. In particular, to relate  $\eta$  to  $\mathcal{M}$ , the mass per unit steradian of the relativistic shell, and  $R$ , the distance traveled before deceleration, requires a good understanding of the radiative transfer and plasma physics of the problem. The value of  $\eta$  is therefore treated as a free parameter, with the limits on the acceptable values of  $\eta$  set by a combination of theoretical and observational constraints. The former is set in this section, while the latter is set in §8.

A specific value of  $\eta$  that has a physical significance is the value of  $\eta$  expected from the continuity equation for a relativistic shock. For  $\Gamma \gg 1$ , one has  $n'_{shell} = n_{ism}\Gamma$ , and

$$\eta_{shock} = \frac{1}{\Gamma}. \quad (2)$$

When  $\eta < \eta_{shock}$ , the interstellar medium density in the shell rest frame is less than the shell density, while it is greater than the shell density when  $\eta > \eta_{shock}$ .

A lower limit  $\eta_{min}$  on  $\eta$  can be derived through a theoretical argument concerning pressure equilibrium within the shell. If one assumes that the interaction with the interstellar medium exerts a force only at the front of the shell, then one can relate  $\eta$  to the temperature of the shell and  $R$ , the distance the shell has traveled from the source when  $\Gamma$  is a factor of 2 below its initial value. This defines a maximum value for the shell density, and therefore a minimum density for  $\eta$ , because when the deceleration force is spread throughout the shell, a lower pressure is required to maintain static equilibrium within the shell. Defining the dimensionless 4-velocity in the radial direction as  $u_r$ , the deceleration of the shell is given by

$$\frac{\mathcal{M}c}{R^2} \frac{du_r}{d\tau} = \Gamma p' = \Gamma n'_{shell,max} T. \quad (3)$$

In this equation, the pressure  $p'$  is the pressure exerted on the shell by the interaction with the interstellar medium as measured in the shell rest frame. The factor of  $\Gamma$  converts this proper measure of force into the radial component of the 4-acceleration. The parameter  $T$  is the sum of the electron and proton temperatures in the shell in units of energy. Changing the derivative on the left-hand side of equation (3) into a derivative in  $r$  and setting  $dr \approx R$  and  $du \approx \Gamma$  gives a maximum density of

$$n'_{shell,max} \approx \frac{\mathcal{M}c^2\Gamma}{2R^3T}. \quad (4)$$

The value of  $R$  in this equation is bounded by a minimum distance  $R_0$  that is set by the case in which the interstellar medium is swept up by the shell. The amount of interstellar medium per unit steradian that must be swept up to change  $\Gamma$  by a factor of 2 is  $m \approx \mathcal{M}/\Gamma$ , so

$$R_0 = \left( \frac{3\mathcal{M}}{m_p n_{ism} \Gamma} \right)^{1/3} = 3.94 \times 10^{-3} \text{ pc } \mathcal{M}_{27}^{1/3} n_{ism}^{-1/3} \Gamma_3^{-1/3}, \quad (5)$$

where  $\mathcal{M}_{27}$  is the shell mass per unit steradians in units of  $10^{27}$  gm,  $n_{ism}$  is given in units of  $\text{cm}^{-3}$ , and  $\Gamma_3$  is the Lorentz factor in units of  $10^3$ . With these parameters, a shell subtending 4 $\pi$  steradians and having  $\mathcal{M}_{27} = n_{ism} = \Gamma_3 = 1$  will carry  $1.129 \times 10^{52}$  ergs of energy, which is the characteristic value inferred from the observations at gamma-ray energies. Using equation (5) to express  $R$  in units of  $R_0$  in equation (4) gives

$$n'_{shell,max} = \frac{m_p c^2 n_{ism} \Gamma^2}{6T} \left( \frac{R_0}{R} \right)^3. \quad (6)$$

The ratio of  $n_{ism}$  to  $n'_{shell}$  is then

$$\eta_{min} = \frac{n_{ism}}{n'_{shell,max}} = \frac{6T}{m_p c^2 \Gamma^2} \left( \frac{R}{R_0} \right)^3. \quad (7)$$

The value of  $\eta_{min}$  is strongly dependent on the distance traveled. For deceleration over  $R = R_0$  with  $T = m_p c^2 \Gamma$ , which is the temperature found when the interstellar medium is swept up adiabatically, one finds  $\eta_{min} \approx \Gamma^{-1} = \eta_{shock}$ , as expected for a shock. For lower values of  $T$ , one has  $\eta_{min} < \eta_{shock}$  unless  $R > R_0$  by a sufficiently large value. For  $T \approx m_e c^2 \Gamma$ , which is the case for the theory discussed below, then one has  $\eta < \eta_{shock}$  for  $R < 6.7 R_0$ . Lower limits on  $\eta$  for  $T = m_e c^2 \Gamma$  and several different values of  $\Gamma$  are given as functions of  $R/R_0$  in Figures 1 and 2.

The value of  $\eta$  defines the light crossing time scale across the shell width. The thickness of the shell in the shell rest frame is related to the mass of the shell by

$$\frac{\mathcal{M}}{R^2} = m_p n'_{shell} l'. \quad (8)$$

Expressing  $R$  in terms of  $R_0$  through equation (5), one finds

$$l' = \left( \frac{\mathcal{M}}{m_p n_{ism}} \right)^{\frac{1}{3}} \left( \frac{\Gamma}{3} \right)^{\frac{2}{3}} \left( \frac{R_0}{R} \right)^2 \eta, \quad (9)$$

$$= 4.05 \times 10^{15} \text{ cm } \mathcal{M}_{27}^{\frac{1}{3}} n_{ism}^{-\frac{1}{3}} \Gamma^{\frac{2}{3}} \left( \frac{R_0}{R} \right)^2 \eta_{-3}. \quad (10)$$

where  $\eta_{-3} = \eta/10^{-3}$ . The thickness of the shell in the interstellar medium rest frame is  $l = l'/\Gamma$ . Defining the shell's characteristic timescale  $t_{shell}$  as  $l = ct_{shell}$ , one has

$$t_{shell} = \frac{\eta}{c} \left( \frac{\mathcal{M}}{9m_p n_{ism} \Gamma} \right)^{\frac{1}{3}} \left( \frac{R_0}{R} \right)^2, \quad (11)$$

$$= 1.35 \times 10^2 \text{ s } \mathcal{M}_{27}^{\frac{1}{3}} n_{ism}^{-\frac{1}{3}} \Gamma^{-\frac{1}{3}} \left( \frac{R_0}{R} \right)^2 \eta_{-3}. \quad (12)$$

For  $\eta$  of order  $1/\Gamma$ , one requires that  $R = 10R_0$  at  $n_{ism} = 1 \text{ cm}^{-3}$  for  $t_{shell} = 1 \text{ s}$ . Equation (12) is plotted in Figures 1 and 2 as functions of  $\eta$  with respect to  $R/R_0$  for several values of  $\Gamma$  and  $t_{shell}$ . Because  $t_{shell}$  must be less than or equal to the burst timescales, which are often observed to be  $< 1 \text{ s}$ , model values for  $\eta$  must be  $\eta \ll 1$ . It is shown in §8 that the theory provides this limit on  $\eta$ .

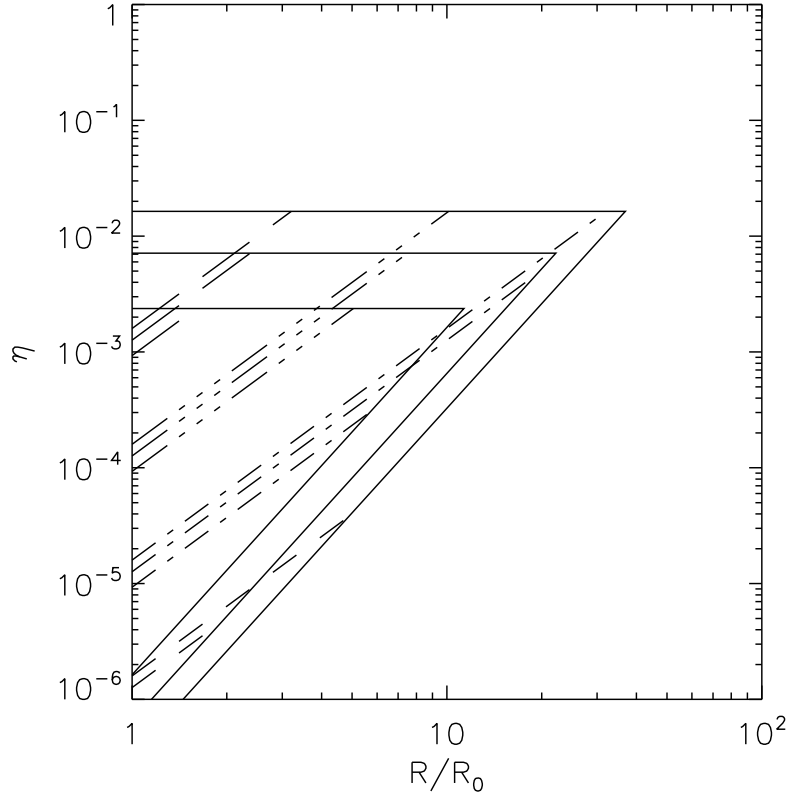


Fig. 1: Limits on  $\eta$ .— The variable  $\eta$  is defined by equation (1) as the ratio of the interstellar medium proper density to the shell proper density. The shell deceleration distance  $R$  is plotted in terms of  $R_0$ , which is defined in eq. (5). Limits on the value of  $\eta$  are plotted as solid curves for the values  $\Gamma = 2 \times 10^3$ ,  $5 \times 10^3$ , and  $10^4$ , with the lower limits given by equation (7), and the upper limits by equation (2). The values of  $\eta$  and  $R$  that produce the shell thickness timescales (eq. [12]) of 0.1 s, 1 s, 10 s, and 100 s, are plotted from bottom to top as a long-dashed, dot-dashed, three-dot-dashed, and long-dashed lines, with a line for each value of  $\Gamma$ , which terminates on the proper boundary for that  $\Gamma$ . Other free parameters were set to  $n_{ism} = 1 \text{ cm}^{-3}$ ,  $\mathcal{M}_{27} = 1$ .

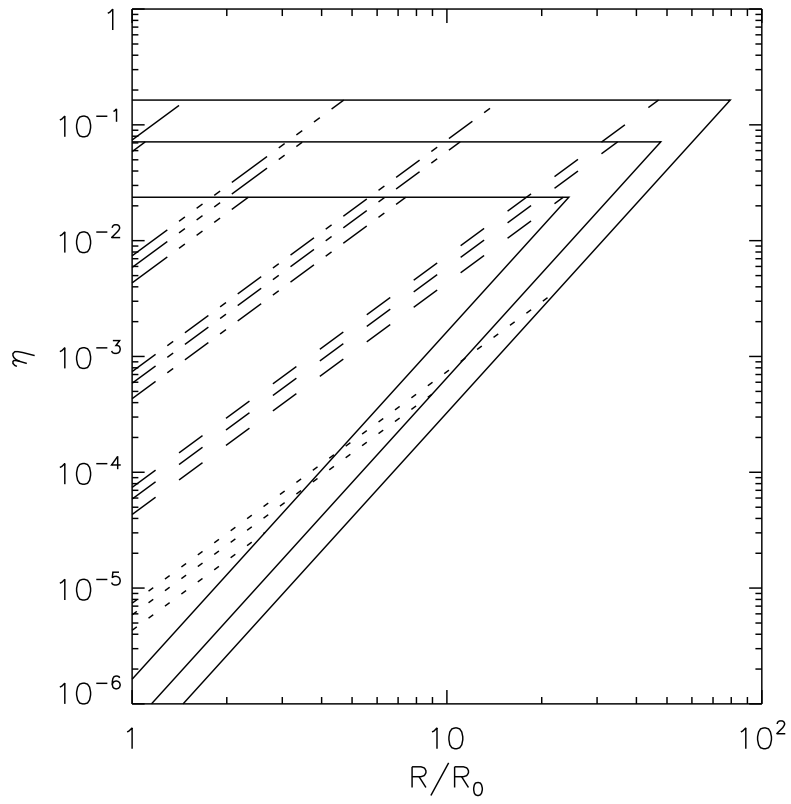


Fig. 2: Limits on  $\eta$ .— The same as Fig. 1, except now  $n_{ism} = 10^5 \text{ cm}^{-3}$ . The dotted-lines at the bottom of the figure are for a shell thickness timescale of 0.01 s, with the remaining curves the same as in Fig. 1.

### 3. Plasma Instabilities

Within the reference frame of the shell, one initially has a plane-parallel charge-neutral density profile through which a neutral and uniform plasma streams. The shell is assumed to have no initial magnetic field. The dissipation of the bulk kinetic energy of a relativistic shell to the interstellar medium must be through a plasma instability, because the densities of the shell and the interstellar medium ensure that the collision mean free path is much longer than the thickness of the shell. For a relativistic plasma, the two relevant instabilities are the two-stream instability and the electromagnetic filamentation instability (Davidson 1990). For  $v \ll c$ , the former has a larger growth rate than the latter by a factor of  $c/v$ , but for  $\Gamma \gg 1$ , the growth rate of the latter becomes much larger than the growth rate of the former.

The two-stream instability has a maximum growth rate in the relativistic regime of

$$\gamma'_{2s} = \frac{1}{2} \omega'_{p,e,ism} \Gamma^{-\frac{3}{2}} \approx \frac{1}{2} \sqrt{\frac{4\pi e^2}{m_e}} n_{ism}^{\frac{1}{2}} \Gamma^{-1}, \quad (13)$$

where  $\omega'_{p,e,ism}$  is the electron plasma frequency of the interstellar medium in the shell rest frame. Taking  $\Gamma = 10^3$  and  $n_{ism} = 1 \text{ cm}^{-3}$ , one finds a growth rate for the electron two-stream instability of  $\gamma'_{2s,e} = 30 \text{ s}^{-1}$  in the shell frame. This growth rate corresponds to distances of travel of  $10^9 \text{ cm}$  for the interstellar medium through the shell.

The filamentation instability acts on counterstreaming plasmas by creating a magnetic pinch. Of the two plasmas, the interstellar medium and the shell, that with the smaller number density in its own rest frame is the plasma that filaments. For gamma-ray bursts, this is the interstellar medium when  $\eta \ll 1$ .

The growth rates of the filamentation instability is easily derived from the dielectric tensor for cold electron and ion streams in the relativistic regime and in the absence of a magnetic field. The equation must satisfy (Davidson 1990)

$$1 + \sum_j \left[ \frac{\omega_{pj}^2}{\Gamma_j^3 c^2 k_{\perp}^2} + \frac{\beta_j \omega_{pj}^2}{\Gamma_j \omega^2} \right] = 0, \quad (14)$$

where  $\omega_{pj}$  is the plasma frequency of component  $j$  for the density measured in the observer's rest frame,  $\Gamma_j$  is this component's Lorentz factor, and  $k_{\perp}$  is the wave number perpendicular to the velocity vector of the streams.

If one is considering only a charge neutral stream of electrons and ions moving with Lorentz factor  $\Gamma$  through a charge neutral background, and if one defines the background plasma to be the shell, then equation (14) gives a frequency of

$$\omega'^2 = - \frac{\beta^2 \left( \omega_{p,e,ism}^{\prime 2} + \omega_{p,i,ism}^{\prime 2} \right)}{\Gamma \left[ 1 + c^{-2} k_{\perp}^{-2} \left( \omega_{p,e,shell}^{\prime 2} + \omega_{p,i,shell}^{\prime 2} \right) \right]}. \quad (15)$$



In this equation,  $\omega'_{p,e,ism}$  and  $\omega'_{p,i,ism}$  are the electron and ion plasma frequencies of the interstellar medium, and  $\omega'_{p,e,shell}$  and  $\omega'_{p,i,shell}$  are the electron and ion plasma frequencies of the shell, all measured in the shell rest frame. The negative value of  $\omega'^2$  shows that the wave grows. Because  $\omega'_{p,e,ism} > \omega'_{p,i,ism}$  and  $\omega'_{p,e,shell} > \omega'_{p,i,shell}$ , one finds that the growth rate of the filamentation of the electrons is

$$\gamma'_{fe} = \frac{\beta\omega'_{p,e,ism}}{\Gamma^{\frac{1}{2}}\sqrt{1 + c^{-2}k_{\perp}^{-2}\omega'_{p,e,shell}{}^2}} \approx \frac{1}{2} \sqrt{\frac{4\pi e^2}{m_e}} n_{ism}^{\frac{1}{2}}. \quad (16)$$

The growth rate is independent of wave length for  $k_{\perp} > \omega'_{p,e,shell}/c$ , and it is  $\propto k_{\perp}$  otherwise. The length scale of the filament is therefore given by  $x_f = k_{\perp}^{-1} = c/\omega_{p,e,shell}$ . For ions alone, the growth rate, which differs from equation (16) only in the numerator, is given by

$$\gamma'_{fi} = \frac{\beta\omega'_{p,i,ism}}{\Gamma^{\frac{1}{2}}\sqrt{1 + c^{-2}k_{\perp}^{-2}\omega'_{p,e,shell}{}^2}} \approx \frac{1}{2} \sqrt{\frac{4\pi e^2}{m_p}} n_{ism}^{\frac{1}{2}}. \quad (17)$$

This has the same length scale as the electron filamentation instability, but a lower growth rate.

The filamentation instability growth rate is faster than the two stream instability by the factor of  $\Gamma$ . For  $\Gamma = 10^3$ ,  $n_{ism} = 1 \text{ cm}^{-3}$ , one finds an electron filamentation growth rate of  $\gamma'_{f,e} = 6 \times 10^4 \text{ s}^{-1}$ , which gives a length scale of  $10^6 \text{ cm}$  over which the instability occurs. For ions, the filamentation instability grows at a rate that is a factor of  $\sqrt{m_e/m_p}$  slower, so that for the parameters given above,  $\gamma'_{f,p} = 1.4 \times 10^3 \text{ s}^{-1}$ . The growth rates of all three instabilities are shown in Figures 3 and 4 as functions of  $\Gamma$ . Both filamentation growth rates are therefore higher than the two-stream growth rate for electrons using the parameters derived above for gamma-ray bursts.

#### 4. Filament Saturation

The filaments grow until the growth rate of the thread equals the magnetic bounce frequency of the particle beam producing the instability (Davidson et al. 1972; Lee & Lampe 1973). The bounce frequency, which describes the motion of a particle across the filament through the toroidal magnetic field, is given by

$$\omega_b = \sqrt{eB/mc\Gamma x_f}, \quad (18)$$

where  $x_f$  is the length scale of the filament, and  $m$  is the mass of the particles comprising the filament. The size of the filaments is set by the lower limit on the wave number for which growth occurs,  $k_{\perp}c = \omega'_{p,e,shell}$ . The ratio of the magnetic field energy density to the particle beam energy density in the thread is then [35]

$$\frac{W'_B}{W'_{ism}} = \frac{m_e n_{ism}}{m n'_{shell}} = \frac{m_e}{m} \eta. \quad (19)$$

One point to note about this equation is that electron and proton components each generate magnetic fields of the same strength. For both components, one has  $W'_B = m_e c^2 n_{ism} \eta \Gamma^2$ , which,

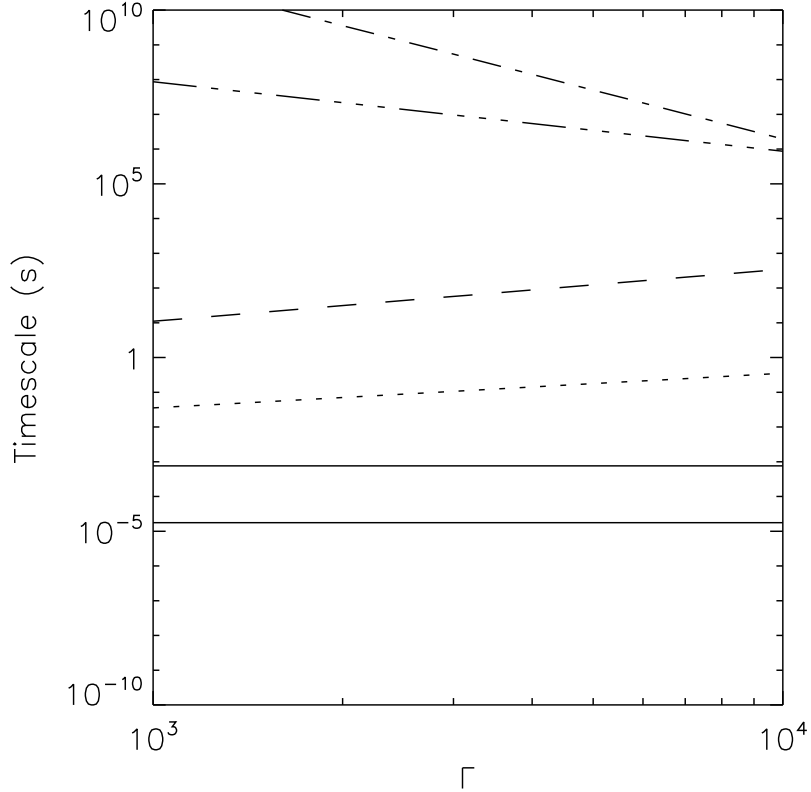


Fig. 3: Timescales.— Instability, radiative, and isotropization timescales versus Lorentz factor. Plasma timescales are given for an ISM plasma density of  $n_{ism} = 1\text{cm}^{-3}$ . The lower two solid curves are the linear growth timescales of the electron and the ion filamentation instabilities,  $t'_{fe}$  and  $t'_{fi}$ . The dotted curve is the timescale for the electron two stream instability. The short dashed curve is the timescale for the electron distribution to isotropize,  $t_{iso}$ . The synchrotron cooling timescale  $t_{sync}$  is given by the line with two dots and one dash, while the synchrotron self-Compton cooling timescale  $t_{Comp}$  is given by the dash and dot line.

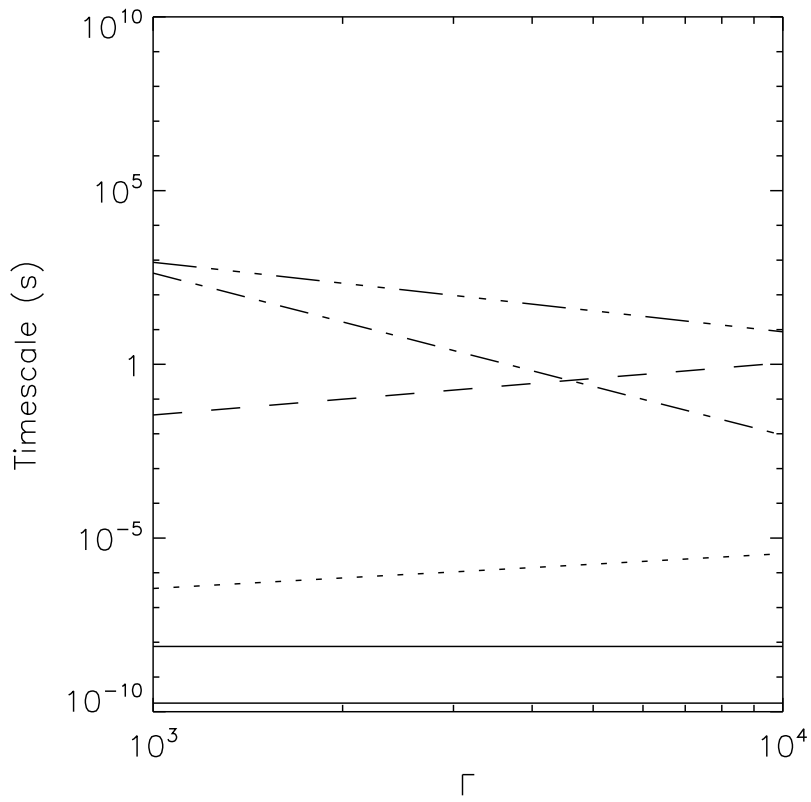


Fig. 4: Timescales.— Instability, radiative, and isotropization timescales versus Lorentz factor. As in Fig. 3, but for  $n_{ism} = 10^5 \text{cm}^{-3}$ .

for  $\Gamma = \eta^{-1} = 10^3$ , gives  $B' = 0.14 G$  with  $n_{ism} = 1 \text{ cm}^{-3}$ , and  $B' = 45.36 G$  with  $n_{ism} = 10^5 \text{ cm}^{-3}$ . This independence is a consequence of the length scale of filamentation being set by the shell electron density.

The thermalization of the ions within the thread can be estimated by examining the equation of motion at saturation. A particle's equation of motion perpendicular to the thread for  $u_x \ll \Gamma$  is (Davidson et al. 1972)

$$\frac{d^2 x}{d\tau^2} = -\omega_b^2 x. \quad (20)$$

Solving this equation of motion using a maximum spatial amplitude of  $x_f$ , one finds that the maximum momentum perpendicular to the filament is  $u_x = x_f \omega_b \Gamma / c$ . Replacing  $x_f$  with the length scale of the filament, and replacing the bounce frequency with the filament growth rate, one finds

$$u_x = \sqrt{\frac{W'_B}{W'_{ism}}} \Gamma. \quad (21)$$

If  $u_x \ll 1$ , then the approximate energy that goes into thermalizing the particles in the stream is approximately given by  $W'_{th}/W'_{ism} = u_x^2/\Gamma$ , while if  $u_x \gg 1$ , it is given by  $W'_{th}/W'_{ism} = u_x/\Gamma$ . As a result,

$$\frac{W'_{th}}{W'_{ism}} = \min\left(\frac{m_e}{m} \eta \Gamma, \sqrt{\frac{m_e}{m} \eta}\right). \quad (22)$$

A point to note is that both of the terms on the right hand side are greater than  $W'_B$ , so that one always has  $W'_{th} > W'_B$ . Equations (19) and (22) are plotted in Figure 5 for  $m = m_p$  and  $\Gamma = 10^3$  and  $10^4$ .

From these equations one sees that the filamentation instability cannot mediate a shock. If a shock were present, then  $\eta$  would be given by equation (2). Placing this equation into equations (19) and (22) and setting  $m = m_p$ , one finds that  $W'_B/W'_{ism} \approx m_e/m_p \Gamma \ll 1$  and  $W'_i/W'_{ism} = (m_e/m_p \Gamma)^{1/2} \ll 1$ . The energy released through the instability is small compared to the kinetic energy of the interstellar medium as measured in the shell rest frame. This contradicts the Rankine-Hugoniot equations, and so a shock never arises through the filamentation instability.

## 5. Electron Thermalization

Once ion filamentation is complete, electrons will attempt to come into equilibrium through the two-stream instability. This instability will drive the electrons to a distribution that is uniformly distributed in energy between the rest frame described by the ions in the filaments and the ions in the shell. The rest frame of the electron distribution must preserve both the electron charge density and the electron current, since the shell plus interstellar medium is charge-neutral. These two conditions define a rest frame for the electrons that has a Lorentz factor relative to the interstellar medium rest frame of

$$\Gamma_e = \frac{\Gamma + \eta}{\sqrt{1 + \eta^2 + 2\eta\Gamma}}. \quad (23)$$

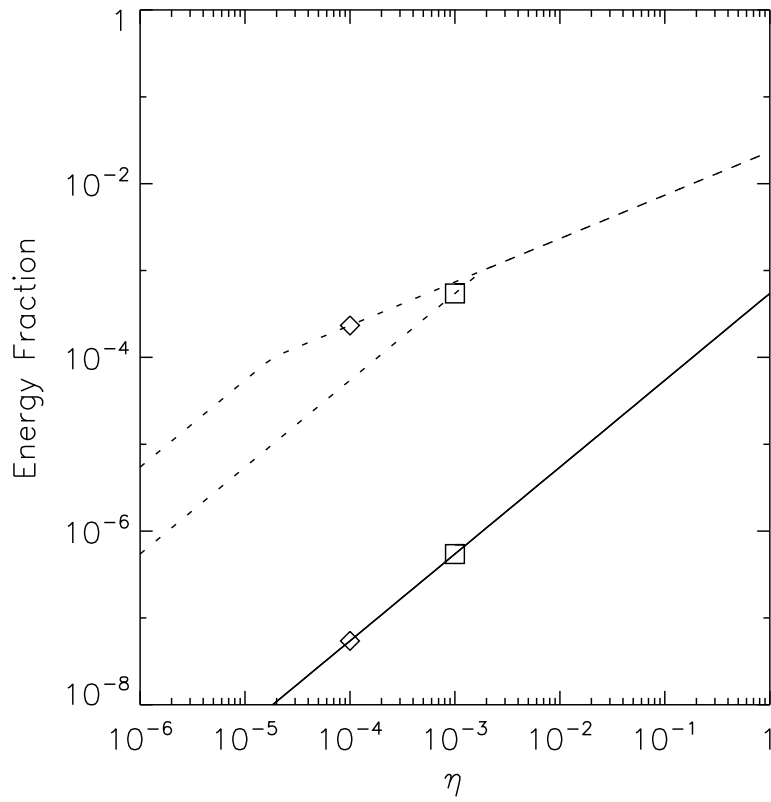


Fig. 5: Energy fractions.— The fraction of the ISM kinetic energy, as measured in the shell rest frame, that goes into magnetic field energy (solid) and ion thermal energy (dotted) for  $\Gamma = 10^3$  and  $10^4$ .

Relative to this rest frame, the shell is moving with

$$\Gamma_s'' = \frac{\eta\Gamma + 1}{\sqrt{1 + \eta^2 + 2\eta\Gamma}}, \quad (24)$$

where the double primes are used to denote quantities measured in the electron rest frame.

In the electron rest frame, the electron density is given by  $n_e'' = n_{ism}\Gamma_e + n'_{shell}\Gamma_s''$ , which can be written as

$$n_e'' = n'_{shell} \sqrt{1 + \eta^2 + 2\eta\Gamma}. \quad (25)$$

The electron rest frame has nearly the same Lorentz factor as the shell rest frame as long as  $\eta \ll \Gamma^{-1}$ . For  $1 \gg \eta \gg \Gamma^{-1}$ , the Lorentz factor of the electrons is  $\Gamma_e = \sqrt{\Gamma/2\eta}$ , which is a factor of  $1/\sqrt{2\eta\Gamma}$  smaller than the Lorentz factor for the ions. The value  $\eta = \Gamma^{-1}$  is therefore an important transition point for the character of the radiation emitted by the shell, because the Lorentz boost of the radiation is smaller than the boost associated with the shell when  $\eta \gg \Gamma^{-1}$ . On the other hand, because  $\eta < 1$ ,  $\Gamma_e'' = \Gamma_e > \Gamma_s''$ , so the two-stream instability drives the electron distribution to the energy defined by  $\Gamma_e$ .

The electron in the shell rest frame has a Landau radius that is much larger than the filament length scale. Using the definitions for  $x_f$ , the gyroradius, and equation (19) for the magnetic field strength in the shell rest frame, one can write

$$\frac{r_e}{x_f} = u_e \frac{m_e}{m_p} \eta. \quad (26)$$

The gyroradius is therefore much larger than the filament width when

$$u_e \gg \frac{m_p}{m_e} \eta. \quad (27)$$

For electrons thermalizing to the energy  $\Gamma_e$ ,  $u_e \approx \Gamma/\sqrt{1+2\eta\Gamma}$ , so that equation (27) becomes

$$\Gamma \gg \begin{cases} \frac{m_p}{m_e} \eta, & \text{if } \eta < \Gamma^{-1}; \\ 2 \left(\frac{m_p}{m_e}\right)^2 \eta^3, & \text{otherwise.} \end{cases} \quad (28)$$

One finds that the inequality holds for the upper term in equation (28) whenever  $\Gamma > \sqrt{m_p/m_e} = 42$ ; below we show that  $\Gamma \gtrsim 10^3$ , so if equation (28) is to fail, it will be for the lower term. For  $\eta\Gamma > 1$ , the inequality holds as long as

$$\eta\Gamma < 2^{-\frac{1}{3}} \left(\frac{m_e}{m_p}\right)^{\frac{2}{3}} \Gamma^{\frac{4}{3}} = 52.9 \Gamma^{\frac{4}{3}}. \quad (29)$$

When inequality (29) holds, each electron passes through many filaments in a single orbit, and the motion of the most energetic electrons will be as a single fluid, but when the inequality fails, the electrons will be confined to the local conditions within each filament, and the motion of each

electron will be determined by these local conditions. For the remainder of the paper, we assume that equation (29) holds.

For the electrons to flow through the magnetic fields generated in the shell, an average electric field perpendicular to the magnetic field must exist in the shell rest frame. The electric field is not uniform, since the system is charge neutral, but exists only over distances of order the width of a filament, with values that are proportional to the magnetic field strength. When the gyroradius is large, the electron effectively sees an average electric field as it completes one orbit. This electric field gives the electron guiding center a velocity of  $-U_s''$  in the shell rest frame. The effective magnetic field strength in the electron rest frame is then

$$B'' = \frac{B'}{\Gamma_s''}. \quad (30)$$

Because the electron travels over many filaments, the orientation of the magnetic field changes dramatically over one gyroradius, so that the direction of the electron's velocity vector is randomized through a random-walk process rather than through the rotation over one orbit. The electron travels the filament width  $x_f$  in the time  $c \delta t''$ . In this time, the angle  $\theta \approx \delta t''/r_e$  is traveled, where  $r_e$  is the electron gyroradius. Because the motion is a random walk, the number of time intervals  $\delta t''$  required to change direction by  $2\pi$  is approximately  $n = 4\pi^2/\theta^2$ . The total amount of time required to isotropize the motion of the electrons is therefore given by

$$t''_{iso} = n\Delta t'' = \frac{4\pi^2 r_e^2}{c x_f} = \frac{4\pi^2 c \Gamma_e^2}{\omega_c''^2 x_f}, \quad (31)$$

where  $\omega_c''$  is the cyclotron frequency. Using equations (19) and (30) to define the magnetic field in equation (31), one finds

$$t''_{iso} = n\Delta t = \frac{2\pi^2 \Gamma_s''}{\omega_{p,e,ism} \eta^{3/2}} = 11.1 \text{ s } n_{ism}^{-\frac{1}{2}} \eta^{-\frac{3}{2}} \frac{\eta \Gamma + 1}{\sqrt{1 + \eta^2 + 2\eta \Gamma}}. \quad (32)$$

For  $\Gamma_s'' \approx 1$ , this timescale is long compared to the two-stream instability for electrons.

## 6. Burst Radiation

Two radiative processes are present within the theory: synchrotron emission and Compton scattering. The synchrotron emission will occur isotropically in the electron rest frame describe by equation (23). The observed synchrotron radiation will be boosted into the observer's reference frame by a factor of  $\Gamma_e$ . Compton scattering of synchrotron radiation by the synchrotron-emitting electrons boosts the radiation by another factor of  $\Gamma_e^2$ , because the electrons in this rest frame have a characteristic energy of  $m_e c^2 \Gamma_e$ .

The characteristic synchrotron frequency in the shell rest frame is given by  $h\nu''/m_e c^2 = 2B''\Gamma_e^2/3B_{cr}$ , where  $B_{cr} = e\hbar/m_e^2 c^3$ . Transforming this into the observer's

reference frame and using equations (19) and (30) to remove  $B''$ , one finds that the characteristic synchrotron energy is

$$\frac{h\nu_s}{m_e c^2} = \frac{2\sqrt{8\pi}\hbar e}{3m_e^{3/2}c^2} \eta^{\frac{1}{2}} n_{ism}^{\frac{1}{2}} \frac{\Gamma_e^3 \Gamma}{\Gamma_s''}, \quad (33)$$

$$= \frac{2\sqrt{8\pi}\hbar e}{3m_e^{3/2}c^2} \eta^{\frac{1}{2}} n_{ism}^{\frac{1}{2}} \frac{(\Gamma + \eta)^3 \Gamma}{(1 + \eta^2 + 2\eta\Gamma)(1 + \eta\Gamma)}, \quad (34)$$

$$= 2.17 \times 10^{-6} \eta_{-3}^{\frac{1}{2}} n_{ism}^{\frac{1}{2}} \frac{\Gamma_3^4}{(1 + 2\eta\Gamma)(1 + \eta\Gamma)}, \quad (35)$$

where terms of order  $\eta$  and higher were dropped in the last equation. Equation (35) places the characteristic energy in the optical band for the given characteristic energies and  $\eta\Gamma < 1$ . As  $\eta$  increases above  $\Gamma^{-1}$ , the characteristic observed energy falls as  $\eta^{-\frac{3}{2}}$ , so  $\eta = \Gamma^{-1}$  defines the maximum characteristic frequency for a given value of  $\Gamma$ . To have a characteristic photon energy of  $m_e c^2$  at  $\eta = \Gamma^{-1}$  requires  $\Gamma > 6.93 \times 10^4 n_{ism}^{-1/7}$ .

The characteristic energy of the Compton emission after a single scattering is a factor of  $\Gamma_e^2$  larger than the synchrotron characteristic energy, so

$$\frac{h\nu_C}{m_e c^2} = \frac{2\sqrt{8\pi}\hbar e}{3m_e^{3/2}c^2} \eta^{\frac{1}{2}} n_{ism}^{\frac{1}{2}} \frac{(\Gamma + \eta)^5 \Gamma}{(1 + \eta^2 + 2\eta\Gamma)^2 (1 + \eta\Gamma)}, \quad (36)$$

$$= 2.17 \eta_{-3}^{\frac{1}{2}} n_{ism}^{\frac{1}{2}} \frac{\Gamma_3^6}{(1 + 2\eta\Gamma)^2 (1 + \eta\Gamma)}. \quad (37)$$

The characteristic energy of the Compton scattered radiation after a single scattering is at  $m_e c^2$  when  $\Gamma > 1.47 \times 10^3 n_{ism}^{1/11}$ . A second scattering takes the photon in the observer rest frame to the GeV energy range. Further scattering does not change the photon energy, because the photon energy is of order the characteristic electron energy after the second scattering.

Each of the radiative components spans a broad range of energies. The low end of the synchrotron emission is set by the cyclotron frequency, which is smaller than the characteristic synchrotron frequency by a factor of  $\Gamma_e^2$ . For  $\eta\Gamma = 1$ , the cyclotron frequency is at  $\nu \approx 2.68 \times 10^8 \text{ Hz } n_{ism}^{1/2} \Gamma_3^{3/2}$ , so that synchrotron emission extends down to the radio band. An important point is that the cyclotron frequency is related to the plasma frequency in the electron rest frame as  $\nu_c'' \approx \sqrt{2}\omega_{p,e}'\eta\Gamma/2\pi(1 + 2\eta\Gamma)^{1/4}$ , so that they are about equal, and the cyclotron photons escape the shell to the observer. The lowest energy of the Compton scattered radiation is the cyclotron frequency photons upscattered by  $\Gamma_e^2$ , which means that the low end of the Compton scattered radiation equals the high end of the synchrotron emission. If most of the energy is in the Compton scattered component, and the synchrotron photon number spectrum falls faster than  $\nu^{-2}$ , so that most of the energy is released at the low end of the spectrum, then the low end of the Compton spectrum will be larger than the high end of the synchrotron spectrum. This implies that optical and ultraviolet emission is part of a single smooth continuum that extends through the x-ray and gamma-ray bands, and that most of the energy emitted by the burst is released in the optical and ultraviolet.



The ratio of the synchrotron emission rate to the single-scattering Compton emission rate for a single electron is given by  $P''_{sync}/P''_{c1} = W''_B/W''_{synch}$ , where  $W''_B$  and  $W''_{synch}$  are the magnetic field and the synchrotron photon energy densities as measured in the electron rest frame. The synchrotron energy density is related to the single electron emission rate by  $W''_{synch} = P''_{synch} n''_{emis} l''/4\pi c$ , where  $n''_{emis}$  is the density of electrons with Lorentz factor  $\Gamma_e$  in the electron rest frame. The synchrotron emission rate is given by  $P''_{sync} = 4\sigma_T c \Gamma_e^2 W''_B/3$ , so the ratio becomes

$$P''_{sync}/P''_{c1} = \frac{3\pi(\eta\Gamma + 1)}{\sigma_T(\Gamma + \eta)^2 f_{emis}} \left( \frac{9m_p}{\mathcal{M}n_{ism}^2 \Gamma^2} \right)^{\frac{1}{3}}, \quad (38)$$

$$= 3.50 \Gamma_3^{-\frac{8}{3}} \frac{(\eta\Gamma + 1) \Gamma^2}{(\Gamma + \eta)^2} n_{ism}^{-\frac{2}{3}} \mathcal{M}_{27}^{-\frac{1}{3}} f_{emis}^{-1} \left( \frac{R}{R_0} \right)^2. \quad (39)$$

The ratio of the synchrotron emission to the rate at which energy carried by the interstellar medium flows through the shell is given by

$$\frac{\dot{E}''_{sync}}{m_p c^3 n_{ion} \Gamma_e^2} = \frac{4m_e \sigma_T \mathcal{M}^{\frac{1}{3}} n_{ism}^{\frac{2}{3}} \Gamma^{\frac{8}{3}} \eta (1 + \eta\Gamma) f_{emis}}{3^{\frac{5}{3}} m_p^{\frac{4}{3}}} \left( \frac{R_0}{R} \right)^2, \quad (40)$$

$$= 1.956 \times 10^{-6} \mathcal{M}_{27}^{\frac{1}{3}} n_{ism}^{\frac{2}{3}} \Gamma_3^{\frac{5}{3}} (\eta\Gamma) (1 + \eta\Gamma) f_{emis} \left( \frac{R_0}{R} \right)^2. \quad (41)$$

For single scattering Compton cooling, this ratio is

$$\frac{\dot{E}''_{Comp}}{m_p c^3 n_{ion} \Gamma_e^2} = \frac{2m_e \sigma_T^2 \mathcal{M}^{\frac{2}{3}} n_{ism}^{\frac{4}{3}} \Gamma^{\frac{10}{3}} \eta (\Gamma + \eta)^2 f_{emis}^2}{3^{\frac{10}{3}} \pi m_p^{\frac{5}{3}}} \left( \frac{R_0}{R} \right)^4, \quad (42)$$

$$= 2.80 \times 10^{-7} \mathcal{M}_{27}^{\frac{2}{3}} n_{ism}^{\frac{4}{3}} \Gamma_3^{\frac{13}{3}} (\Gamma\eta) \frac{(\Gamma + \eta)^2}{\Gamma^2} f_{emis}^2 \left( \frac{R_0}{R} \right)^4. \quad (43)$$

From these equations, one sees that the energy release is very inefficient unless  $n_{ism}$  or  $\Gamma$  are larger than the characteristic values used in the calculations. We discuss this point in §8.

## 7. Radiative Timescales

The cooling time scale for synchrotron emission of a relativistic electron is found by dividing the electron energy  $m_e c^2 \Gamma_e$  by  $P''_{sync}$ , the emissivity of a single electron. In the electron rest frame, the synchrotron cooling timescale is

$$t''_{sync} = \frac{3}{4\sigma_T c \eta n_{ism}} \frac{(\eta\Gamma + 1)^2}{\Gamma^2 (\Gamma + \eta) \sqrt{1 + \eta^2 + 2\eta\Gamma}}, \quad (44)$$

$$= 3.76 \times 10^7 \text{ s } n_e^{-1} \Gamma_3^{-2} \frac{(\eta\Gamma + 1)^2}{\eta (\Gamma + \eta) \sqrt{1 + \eta^2 + 2\eta\Gamma}}. \quad (45)$$

The synchrotron self-Compton cooling timescale is found by multiplying equations (38) and (45) together, which gives

$$t''_{Comp} = \frac{9\pi}{4\sigma_T^2 c f_{emitt} n_{ism}} \left( \frac{9m_p}{n_{ism}^2 \mathcal{M}} \right)^{\frac{1}{3}} \frac{(\eta\Gamma + 1)^3}{\eta\Gamma^{\frac{8}{3}} (\Gamma + \eta)^3 \sqrt{1 + \eta^2 + 2\eta\Gamma}} \left( \frac{R}{R_0} \right)^2, \quad (46)$$

$$= 1.32 \times 10^8 \text{ s } \mathcal{M}_{27}^{-\frac{1}{3}} n_{ism}^{-\frac{5}{3}} f_{emitt}^{-1} \Gamma_3^{-\frac{14}{3}} \frac{(\eta\Gamma + 1)^3 \Gamma^2}{\eta (\Gamma + \eta)^3 \sqrt{1 + \eta^2 + 2\eta\Gamma}} \left( \frac{R}{R_0} \right)^2. \quad (47)$$

These timescales are plotted in Figures 3 and 4 for  $n_{ism} = 1 \text{ cm}^{-3}$  and  $10^5 \text{ cm}^{-3}$ , with  $(R/R_0)^2 = m_p/m_e$ , and  $\eta\Gamma = 1$ . One sees that for the higher densities, the Compton cooling timescale can fall below the timescale for isotropization. When this occurs, the radiative cooling will determine the shape of the electron distribution. The Compton cooling timescale is shorter than the isotropization timescale when

$$n_{ism} > 1.16 \times 10^6 \text{ cm}^{-3} \left( \frac{R}{R_0} \right)^{\frac{12}{7}} \Gamma_3^{-\frac{37}{7}} \left[ \frac{\eta^{\frac{1}{2}} \Gamma^{\frac{7}{2}} (\eta\Gamma + 1)^2}{(\Gamma + \eta)^3} \right]^{\frac{6}{7}}. \quad (48)$$

## 8. Observational Consequences

The theory outlined above has within it two observational selection effects that define lower limits on the values of  $n_{ism}$  and  $\Gamma$ . These selection effects arise because gamma-ray bursts are recognized as such through the efficient emission of gamma-rays.

Because gamma-ray bursts are selected by their gamma-ray emission, one must have a value of  $\eta$  that is sufficiently small to give gamma-rays through Compton scattering. Because the largest value of the photon energy occurs at  $\eta = 1/\Gamma$ , one can derive a lower limits on  $\Gamma$  by requiring the right hand side of equation (37) be  $> 1$  at this value of  $\eta$ :

$$\Gamma_3 > 0.831 n_{ism}^{-\frac{1}{11}}. \quad (49)$$

The weak dependence on  $n_{ism}$  implies that for all gamma-ray bursts, the bulk Lorentz factor  $\Gamma > 10^3$ . Events may occur with smaller  $\Gamma$ , but these would emit in the optical and ultraviolet bands.

From Figures 6 and 7, one sees that an upper limit on the value of  $\eta$  is found from equation (37) for  $\eta\Gamma \gg 1$ . This limit is

$$\eta < \eta_{max} = 1.03 \times 10^{-3} n_{ism}^{\frac{1}{5}} \Gamma_3^{\frac{6}{5}}. \quad (50)$$

These upper limits are plotted in Figures 1 and 2. An important aspect of these limits is that the timescales associated with the shell thickness are generally  $< 1$  s. For the higher density figure, the time scales at  $R/R_0 = 0.1$  range from 0.01 s to 1 s, which is consistent with the shortest timescales exhibited by gamma-ray bursts.

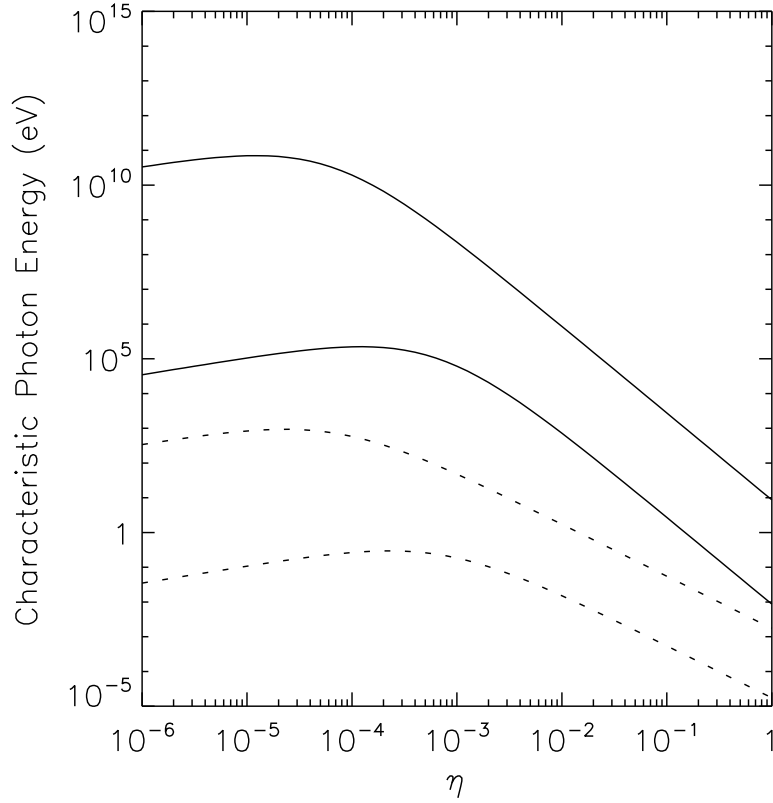


Fig. 6: Characteristic radiation energies.— The characteristic synchrotron emission (dotted lines) and synchrotron self-Compton emission (solid lines) energies of photons emitted from the relativistic shell as measured by an observer at rest in the interstellar medium for photons emitted along the velocity vector of the shell. Values of  $\Gamma = 10^3$  (upper curves) and  $10^4$  (lower curves) are used. The density is  $n_{ism} = 1 \text{ cm}^{-3}$ .

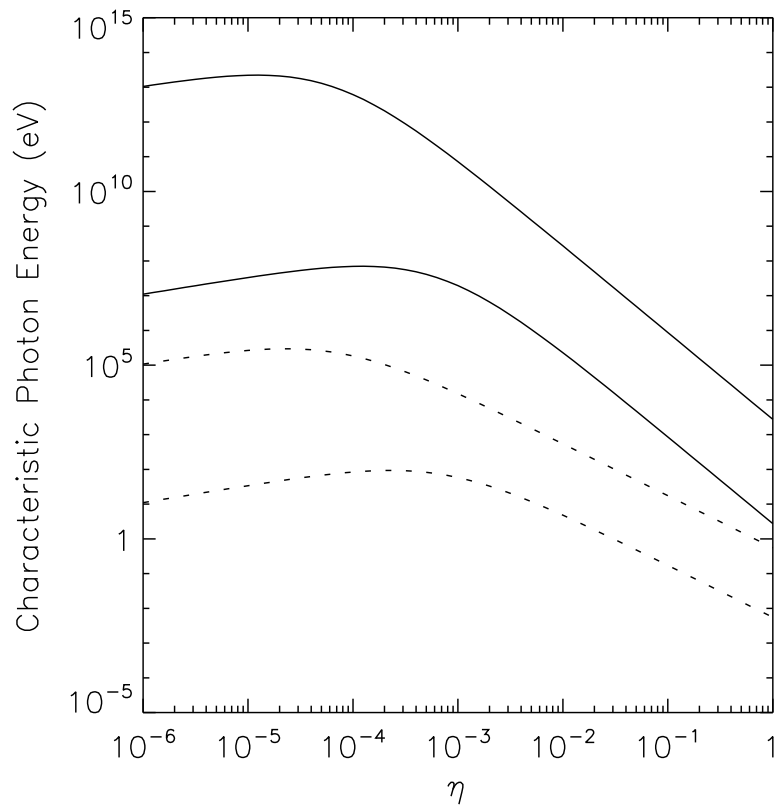


Fig. 7: Characteristic radiation energies.— Same as Fig. 6, but for  $n_{ism} = 10^5 \text{ cm}^{-3}$ .

Lower limits on the interstellar medium density are found by requiring that Compton scattering efficiently remove energy from the shell. Two conditions must be met: first, Compton cooling must dominate synchrotron cooling, and second, the Compton cooling rate must be comparable to the rate at which energy is lost as the shell decelerate over the distance  $R$ . The first of these conditions is derived from equation (39):

$$n_{ism} > 6.54 \mathcal{M}_{27}^{-\frac{1}{2}} f_{emis}^{-\frac{3}{2}} \frac{(\eta\Gamma + 1)^{\frac{3}{2}} \Gamma^3}{(\Gamma + \eta)^3} \Gamma_3^{-4} \left( \frac{R}{R_0} \right)^3. \quad (51)$$

The second of these conditions is found by equating the right hand side of equation (43) to  $(R_0/R)^3 g$ , where  $g \leq 1$  is a measure of efficiency. This gives

$$n_{ism} = 8.22 \times 10^4 \text{ cm}^{-3} \mathcal{M}_{27}^{-\frac{1}{2}} \Gamma_3^{-\frac{13}{4}} f_{emis}^{-\frac{3}{2}} \left( \frac{R}{R_0} \right)^{\frac{3}{4}} g^{\frac{3}{4}}. \quad (52)$$

If  $g$  is very small in equation (52), then most of the energy lost by the shell to the interstellar medium is not radiated away, making the burst dim and unobservable.

The limits from equations (51) and (52) on  $n_{ism}$  are plotted as functions of  $\Gamma$  in Figure 8. The point to note in this figure is that the density required for high efficiency cooling is very high, of order  $10^5 \text{ cm}^{-3}$ . This is important in explaining why all gamma-ray bursts have a peak value of the  $\nu F_\nu$  curve near 250 keV. The high source density provides a medium for Compton attenuation of the burst spectrum. Because the scattering medium is at rest in the galaxy rest frame, the value of  $E_p$  is independent of  $\Gamma$ , even though the characteristic energy emitted by the shell is a strong function of  $\Gamma$ . As a consequence, if the medium density is low enough to keep attenuation from occurring, then the density will be too low to efficiently produce gamma-ray emission. In such a circumstance, the shell will loose energy by thermalizing ions and electrons, but the thermal energy of the electrons will not be rapidly radiated away, making these particular sources invisible.

An interesting consequence of the density on the theory is that as the density increases, the timescale for radiative cooling becomes shorter than the timescale for isotropization of the electron distribution. The implications of this is that there should be a coupling of the electron distribution to the density of the interstellar medium, with the distribution falling more rapidly, and being more anisotropic, at the higher interstellar medium densities. Because the shape of the electron distribution determines the shape of the spectrum, one expects the burst spectrum to become softer for the higher interstellar medium densities, and therefore for the higher attenuation optical depths. This is the case observationally, so this theory may provide an explanation for that one characteristic of the Compton attenuation theory.

The theory as constructed has two natural timescales, one from the thickness of the shell, and the second from the deceleration distance  $R$ . The shell thickness timescale is given by equation (12), and is of order 2.9 s for  $n_{ism} = 10^5 \text{ cm}^{-3}$  and  $R/R_0 = 1$ . For the same density and  $R/R_0 = 10$ ,

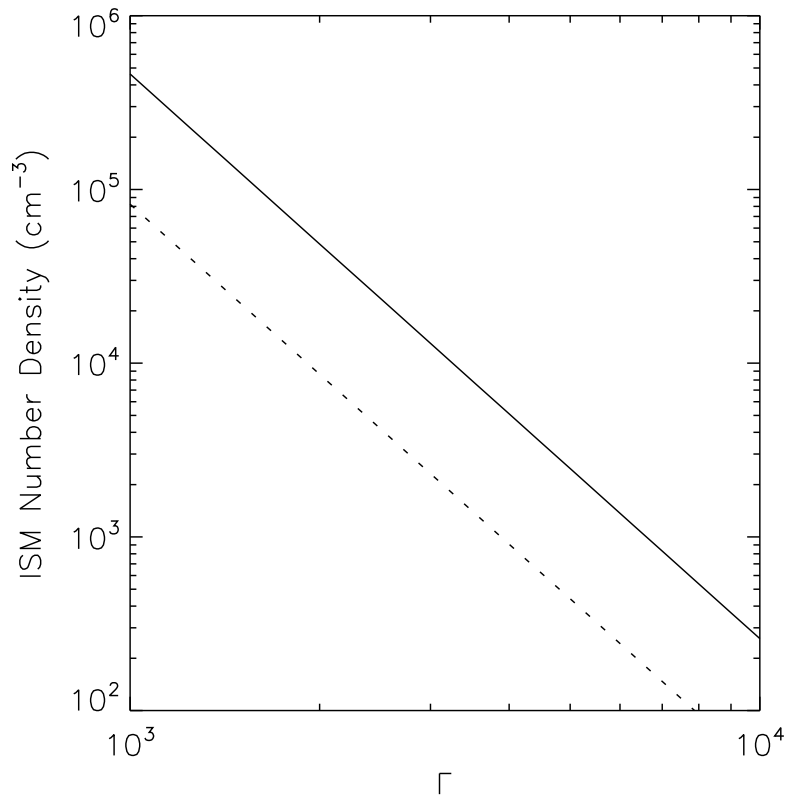


Fig. 8: Limits on density.— The lower limits on  $n_{ism}$  as a function of  $\Gamma$ .

the timescale falls to 0.029 s. The deceleration timescale is given by

$$t_R = \frac{R}{2c\Gamma^2} = 0.203 \text{ s } \mathcal{M}_{27}^{1/3} n_{ism}^{-1/3} \Gamma_3^{-7/3} \left( \frac{R}{R_0} \right), \quad (53)$$

where the definition of  $R_0$  in equation (5) has been used. This timescale is less than the shell thickness timescale whenever

$$\frac{R}{R_0} > 8.74 \Gamma_3^{2/3} \eta_{-3}^{1/3}. \quad (54)$$

Because  $\frac{R}{R_0}$  should be of order  $m_p/m_e$ , the two timescales are of the same order. When the two timescales are equal, the value is given by

$$t_R = t_{shell} = 1.77 \text{ s } \mathcal{M}_{27}^{1/3} n_{ism}^{-1/3} \Gamma_3^{-5/3} \eta_{-3}^{1/3}. \quad (55)$$

For  $n_{ism} = 10^5 \text{ cm}^{-3}$ , the timescale is 0.038 s. The timescales associated with both the shell and the deceleration distance are sufficiently short to be responsible for the shortest timescales observed in gamma-ray bursts.

## 9. Summary of Conclusions

To summarize the theory presented above, a baryonic shell with an ultra-relativistic bulk velocity interacts with the interstellar medium through the filamentation and the two-stream plasma instabilities. The former instability gives rise to a magnetic field with a strength that is far below the equipartition value, and the latter instability heats the electrons to energies that are relativistic, but also far below the equipartition value. Neither instability is sufficient to produce a shock. Instead, the interstellar medium passes through the shell, so that the region behind the shell is not cleared of interstellar medium. The electrons within the shell produce synchrotron radiation with a characteristic energy in the observer's rest frame that ranges from the radio to the ultraviolet. Synchrotron self-Compton emission by the electrons in the shell produces x-rays and gamma-rays in the observer's rest frame, in addition to optical emission. The optical emission is dominated by the synchrotron self-Compton component. The timescales associated with the shell thickness and the length scale over which the shell decelerates provide a lower limit on the burst durations. The burst duration itself would be determined by the complex structure of the relativistic wind, since the interstellar medium remains in place, permitting multiple shells to each produce gamma-ray emission.

Two conditions must be met for the interaction between shell and interstellar medium to efficiently produce gamma-rays: first, the bulk Lorentz factor must be  $> 10^3$  in order to produce radiation above 1keV; second, the number density of the interstellar medium must be greater than  $\approx 10^6 \text{ cm}^{-3} \Gamma_3^{-13/4}$ , where  $\Gamma_3$  is the bulk Lorentz factor in units of  $10^3$ , for the thermal energy to be radiated efficiently. The lower limit on  $\Gamma$  through the selection effect provides an explanation for why the value of  $\Gamma$  is always sufficiently high to allow the escape of 1MeV photons from the

gamma-ray burst emission region without the production of an electron-positron plasma from photon-photon pair creation and the subsequent thermalization of the radiation. The limit on density provides an explanation of why all gamma-ray burst spectra appear to be Compton attenuated. Because the limits on  $\Gamma$  and  $n_{ism}$  are from selection effects in observing the emission of gamma-rays, one expects there to be burst events with values of  $\Gamma$  and  $n_{ism}$  outside these limits. For bursts with low  $\Gamma$ , the bursts radiate at energies below 1 keV. Therefore, one expects a population of optical and ultraviolet transients that have no gamma-ray emission. For bursts with low density, the radiation of energy is inefficient, so that the bursts are of low intensity. These bursts may appear in burst samples through a correlation of burst intensity with the interstellar medium density inferred from the Compton attenuation model.

An aspect of the theory that provides a test is the comparison of instantaneous gamma-ray, x-ray, and optical emission to the radio and optical emission. There are two aspects of the theory to test. First, one can test whether the broad band spectrum is consistent with being a synchrotron spectrum at low frequency and a Compton scattered synchrotron spectrum at higher frequency. Second, one can test the consistency of physical parameters in the theory. This last is done by comparing the Thomson and photoelectric optical depths found through a fit of the Compton attenuation model to the optical attenuation derived under the assumption that the unattenuated gamma-ray continuum extends to the optical band. Third, if the optical spectrum is sufficient to fix the cyclotron frequency by determining the low energy drop-off of the Compton spectrum, one can solve for the value of the Lorentz factor, which will provide a consistency test through the lower limit on  $\Gamma$ . If one can model the x-ray afterglow of a burst as the forward scattering of x-rays by dust, then one has additional information about the optical extinction that can be used in this comparison.

The theory of afterglows in this theory has yet to be developed. An important difference from the shock theory of afterglows is that the region behind the shell will emit afterglow radiation in competition with the radiation from the decelerated shell. Because the evolution of the afterglow from the interstellar medium is determined by the broadening of the look-back surface and the radiative cooling of the interstellar medium, while the evolution of the shell radiation is determined by the decrease in  $\Gamma$  and the evolution of the thermal structure of the shell, the theory should have two distinct afterglow components that produce a complex afterglow behavior.

Numerical modeling of the plasma processes can lead to additional observational tests of the theory. In particular, the numerical modeling of the electron distribution for the regime where the electron isotropization timescale exceeds the Compton cooling timescale (Fig. 2) may provide a test through the correlation of Thomson optical depth with spectral hardness. One suspects that as  $\Gamma$  increases, the synchrotron spectrum becomes softer, because an electron radiatively cools before it isotropizes, making the electron distribution one-dimensional. Because of the lower limit on  $n_{ism}$  in inversely related to  $\Gamma$ , one expects  $n_{ism}$ , and therefore the Thomson optical depth, to be smaller for softer spectra. This conjecture requires numerical verification; if it is verified, then one can use the correlation of unattenuated spectral index with Thomson optical as a test of the



theory. There is already some evidence of such a correlation (Brainerd et al. 1998, Fig. 8a).

Two theoretical investigations are now warranted. The first is a study of the broad band spectrum expected for this theory need to be numerically calculated for a number of electron distributions. This study will determine what aspects of the spectrum provide tests of the theory without requiring a full understanding of the plasma processes. Such a study can be carried out through Monte Carlo simulation, and should include the effects of optical and Compton attenuation. The goal is to model the spectrum from the radio to the gamma-ray. The second is a study of the plasma processes. This will require the development of plasma codes to study the interactions of relativistic beams and the growth of instabilities to the nonlinear regime. Only such a study will verify if the analytic conclusions reached above are accurate. Only such a study will one determine the value of  $\eta$  in terms of the other burst parameters. And only through such a study will one obtain model spectra that are dependent just on the bulk Lorentz factor, the density of the interstellar medium, and the mass of the relativistic shell.

The plasma instability theory is capable of explaining the most important features of gamma-ray bursts. Further theoretical research is therefore justified, and should lead to strong and unambiguous observational tests of the theory.

## REFERENCES

- Baring, M. G., & Harding, A. K. 1996, in *AIP Conf. Proc. 384: Gamma-ray Bursts, 3rd Huntsville Symposium*, ed. C. Kouveliotou, M. S. Briggs, & G. J. Fishman (New York: AIP), 724
- Brainerd, J. J. 1994, *ApJ*, 428, 21
- Brainerd, J. J. 1996, in *Gamma-ray Bursts: Third Symposium, Huntsville, AL 1995*, ed. C. Kouveliotou, M. S. Briggs, & G. J. Fishman (New York: AIP), 148
- Brainerd, J. J., Preece, R. D., Briggs, M. S., Pendleton, G. N., & Paciesas, W. S. 1998, *ApJ*, 501, 325
- Brainerd, J. J., Pendleton, G. N., Mallozzi, R., Briggs, M. S., & Preece, R. D., 1999, *ApJ*, in preparation
- Davidson, R. C. 1990, “Physics of Nonneutral Plasmas” (Redwood City: Addison-Wesley)
- Davidson, R. C., Hammer, D. A., Haber, I., & Wagner, C. E. 1972, *Phys. Fluids*, 15, 317
- Djorgovski, S. G., Kulkarni, S. R., Goodrich, R., Frail, D. A., & Bloom J. S. 1998, *GCN Circ.* 137
- Djorgovski, S. G., Kulkarni, S. R., Goodrich, R., Frail, D. A., & Bloom J. S. 1998, *GCN Circ.* 139
- Djorgovski, S. G., Kulkarni, S. R., Bloom, J. S., Frail, D., Chaffee, F. & Goodrich, R. 1999, *GCN Circ.* 189
- Fruchter, A. S. 1999, *ApJ*, 512, L1

- Kelson, D. D., Illingworth, G. D., Franx, M., Magee, D., & van Dokkum, P. G. 1999, *IAU Circ.* 7096
- Kulkarni, S. R., et al. 1998, *Nature*, 393, 35
- Lee, R., & Lampe, M. 1973, *Phys. Rev. Lett.*, 31, 1390
- Mallozzi, R. S., et al. 1996, in *AIP Conf. Proc. 384: Gamma-ray Bursts, 3rd Huntsville Symposium*, ed. C. Kouveliotou, M. S. Briggs, & G. J. Fishman (New York: AIP), 204
- Mészáros, P. 1998, in *AIP Conf. Proc. 428: Gamma-ray Bursts, 4rd Huntsville Symposium*, ed. C. A. Meegan, R. D. Preece, & T. M. Koshut (New York: AIP), 647
- Metzger et al. 1997, *IAU Circ.* 6655
- Metzger, R. M., Djorgovski, S. G., Kulkarni, S. R., Steidel, C. C., Adelberger, K. L., Frail, D. A., Costa, E., & Frontera, F., 1997, *Nature*, 387, 878
- Mochkovitch, R., & Daigne, F. 1998, in *AIP Conf. Proc. 428: Gamma-ray Bursts, 4rd Huntsville Symposium*, ed. C. A. Meegan, R. D. Preece, & T. M. Koshut (New York: AIP), 667
- Piran, T., & Sari, R. 1998, in *AIP Conf. Proc. 428: Gamma-ray Bursts, 4rd Huntsville Symposium*, ed. C. A. Meegan, R. D. Preece, & T. M. Koshut (New York: AIP), 662
- Preece, R. D., & Brainerd, J. J. 1999, *ApJ*, in preparation
- Preece, R. D., Briggs, M. S., Mallozzi, R. S., Pendleton, G. N., Paciesas, W. S., & Band, D. L. 1998a, in *AIP Conf. Proc. 428: Gamma-ray Bursts, 4rd Huntsville Symposium*, ed. C. A. Meegan, R. D. Preece, & T. M. Koshut (New York: AIP), 319
- Preece, R. D., Briggs, M. S., Mallozzi, R. S., Pendleton, G. N., Paciesas, W. S., & Band, D. L., 1998b *ApJ*, 506, L23
- Preece, R. D., Briggs, M. S., Pendleton, G. N., Paciesas, W. S., Matteson, J. L., Band, D. L., & Meegan, C. A. 1996, *ApJ*, 473, 310
- Rees, M. J., & Mészáros, P. 1992, *MNRAS*, 258, 41P
- Rees, M. J., & Mészáros, P. 1994, *ApJ*, 430, L93
- Schmidt, W. K. H. 1978, *Nature*, 271, 525
- Tavani, M. 1996, *ApJ*, 466, 768